Short Communication

Influence of Sodium Lignosulfonate on the Corrosion-Inhibition Behavior of Q235 Steel in Simulated Concrete Pore Solutions

Jiansan Li, Weilin Liu[*], Wanchen Xie

School of Mechanical and Automotive Engineering, South China University of Technology, Guangzhou 510640, People's Republic of China
[*]E-mail: 201821003510@mail.scut.edu.cn

The corrosion mechanism and behavior of Q235 steel treated with sodium lignosulfonate and a mixture of sodium lignosulfonate and sodium silicate inhibitors in simulated concrete pore (SCP) solutions containing 0.08-mol/L NaCl were evaluated using polarization methods, electrochemical impedance spectroscopy, scanning electron microscopy, weight-loss measurements, and potential-of-zero-charge analysis. Results verified that the inhibition efficiency rapidly increased as the sodium lignosulfonate content increases, and the adsorption process mainly comprised chemisorption. The optimum sodium lignosulfonate concentration was 0.0015 mol/L. Sodium lignosulfonate and sodium silicate showed a synergistic inhibition effect in SCP solutions, with the highest inhibition efficiency of 98.8% achieved when 0.0005-mol/L sodium lignosulfonate and 0.0005-mol/L sodium silicate were used.

1. INTRODUCTION

Concrete is widely used in infrastructure construction around the world because of its low price and durability [1]. The main factor influencing infrastructure degradation is the corrosion of steel bars. In developed countries , the cost of infrastructure corrosion maintenance accounts for approximately 3% of the gross domestic product [2]. Corrosion rates are greatly accelerated when the buildings are exposed to weather conditions such as high temperatures, humidity, or marine environments. Erosion by chloride ions and concrete carbonation lead to the destruction of the protective layer on the metal surface [3]. The continuous penetration of Cl^- and CO_2 can cause the steel to rapidly crack. This does not only causes hazards but also brings huge economic losses. To avoid corrosion-related degradation, the methods used to mitigate the corrosion rate of steel include electrochemical cathodic protection and electrochemical realkaliation as well as the use of modified stainless steel, anti-corrosion coatings, and corrosion

inhibitors [4, 5]. Corrosion inhibitors are extensively applied because of their handy, low budget, and enhanced inhibition performance. The ways in which an inhibitor can delay corrosion are (i) by strengthening the passive film on carbon steel to reduce the rate of chlorides ingression; (ii) by reacting with chlorides in concrete; (iii) by eliminating the oxygen dissolved in the pore solution; (iv) by raising the chloride threshold level; (v) by reducing the rate of corrosion at the onset of the process [6-8]. According to the chemical composition of inhibitors, these fall into two categories: (i) inorganic inhibitors, such as nitrite, molybdate, and tungstate [9, 10]; (ii) organic inhibitors, including amino-alcohol-based inhibitors, deoxyribonucleic acid, coconut leaf extract, solanum lasiocarpum L. extract, and furocoumarin derivatives [11-15]. Most of the traditional inorganic inhibitors are toxic, so researchers have recently focused their attention on green, biodegradable corrosion inhibitors [16-21].

Lignin is one of the essential components found in the cell wall of lignocellulosic fibers. Among the renewable biopolymers, its natural high polymer is only subordinate to cellulose [22] and it is also a sustainable and high-quality raw material for the aromatic chemicals and fuels production [23]. Lignin can chelate with metal ions through coordination bonds because it contains several oxygen-containing functional groups such as carboxyl, phenolic hydroxyl, and methoxy [24]. In addition, lignin is cheap and degradable, so it is frequently used to absorb heavy metals [25].

Lignosulfonate is a lignin derivative that contains hydrophilic (sulfonic and alcohol hydroxyl) groups as well as hydrophobic (carbon chain) groups. Due to its unique performance, it has a wide range of applications, for example, as concrete water reducer, surfactant, refractory, and so on [26, 27]. Nearly 50 million tons of lignosulfonate are produced every year during pulping of paper [28]. Direct discharge would be a resource waste and would cause environmental pollution, so the reuse of lignosulfonate has become an urgent problem to be solved. Lignosulfonate is an anionic surfactant with surface activity [29]. It is not only able to promote adsorption of material but can also make particles disperse further, subsequently forming a film on a metal surface. Thus, it has a potential for applications in corrosion and scale inhibitions [30]. In acid solution, the inhibition performance of lignin derivatives on carbon steel depends on the amount of carboxyl, the concentration of inhibitor, and the environment. In the case of solutions containing Cl^- ions, functional groups exert an enormous effect on the inhibition efficiency of lignin derivatives [31].

Sodium lignosulfonate contains large amounts of hydroxyl, carboxyl, or methoxy groups that provide lone pairs of electrons or π-electrons. A d_{sp} empty orbitals of metal coordinates with these electrons [32, 33], which adsorb on the surface of metal and generate a protective film to block the invasion of corrosive medium [34]. The carboxyl and sulfonate groups of sodium lignosulfonate, which are negatively charged, adsorb on carbon steel and easily disperse $CaCO_3$, so this compound can be used as a scale inhibitor for circulating cooling water [35].

Sodium silicate (Na_2SiO_3)—commonly known as "water glass"— not only shows good chemical and thermal stability but also is biocompatible and environment-friendly; therefore, it is commonly used as a metal coating or corrosion inhibitor [36],[37]. Since the 1950s, silicate has been employed in cooling water systems for inhibiting the corrosion behavior of stainless steel [38]. The existence of SiO_3^{2-} results in the formation of two precipitation layers. Iron is the main component of the inner layer's corrosion product. A mixture comprising silicon dioxide, ferrous hydroxide, and silica gel is adsorbed on the outer layer [39, 40]. In addition, silicate coatings on galvanized steel and aluminum and magnesium alloys

have been extensively studied [31, 41, 42]. In the case of aluminum alloy, silicate is used as a cleaner for pretreatment and as a corrosion inhibitor [43]. Silicate is used to prevent zinc from corroding as follows: $Si_2O_5^{2-}$ gathers and preferentially deposits on the passive film to improve self-healing performance on the coating, so silicate is conducive for pitting corrosion protection [35].

In this study, the inhibition performance of sodium lignosulfonate on Q235 steel in an SCP solution containing 0.08-mol/L NaCl is investigated for the first time by electrochemical techniques, scanning electron microscopy (SEM), weight-loss measurements, and zero-potential charge analysis. Moreover, concrete contains silicate, which is an environmentally friendly inhibitor and is effective in high-chloride environments. During the hydration process of Portland cement, C–S–H gel is produced. Considering the existence of a C–S–H gel, we evaluated the synergistic inhibition effects and corrosion-inhibition mechanisms of a mixture of sodium lignosulfonate and sodium silicate.

2. EXPERIMENTAL

2.1 Materials and sample preparation

Q235 carbon steels were used for all experiments. The main elements (mass fraction) of the material was: 0.13% C, 0.002% S, 0.17% Si, 0.57% Mn, 0.021% P, 0.11% O, 0.003% N, and Fe (balance). Steel bars were fabricated into cylinders with 12-mm diameter and 30-mm length for the electrochemical test. Brass wires were fixed on one end of the samples using a conductive adhesive. Carbon steels were placed with the interior of PVC pipe. All parts—except the working surface—were sealed using an epoxy resin. After being completely solidified, the working surface was ground in a stepwise manner using metallographic paper from W28 to W7. The surface was then scrubbed with alcohol, rinsed by ultrapure water, and desiccated below 70°C in an oven. For the surface morphology analysis, steels with Φ12-mm diameter and 10-mm long were successively polished by series sandpaper (from W28 to W3.5) and burnished with a metallographic polishing agent, followed by ultrasonic cleaning in ethanol and drying. Samples with a size of $50 \times 25 \times 2$ mm^3 were prepared for the weight-loss measurements.

A saturated calcium hydroxide solution containing 0.08-mol/ L NaCl served as the SCP solution. Its pH value was approximately 12.5. The concentrations of sodium lignosulfonate were 0.0001, 0.0005, 0.001, and 0.0015 mol/L. A mixture of sodium lignosulfonate (0.0005 mol/L) and sodium silicate (0.0005 mol/L) was applied to the SCP solution as a composite corrosion inhibitor. Ultrapure water was used as a solvent.

2.2 Experimental methods

2.2.1 Potentiodynamic polarization measurements

All electrochemical measurements were performed on a Princeton 263A electrochemical workstation. A three-electrode system, including a saturated calomel electrode as the reference electrode, a platinum electrode as the auxiliary electrode with an area of 20 mm × 20 mm, and the Q235 steel as the working electrode, was employed. The surface area of the steel sample was approximately 1 cm^2. In

advance of each electrochemical measurement, open-circuit potential (OCP) experiment was conducted, and the sample was exposed to the testing solution for 40 min to obtain a steady state. To ensure the removal of oxides on working surface, a constant potential of -1.0 V was applied to the samples for 600 s. The potentiodynamic polarization curve was recorded from the cathodic direction, which was negatively shifted by 250 mV from the OCP, to the anodic direction until 1 V. The scan rate was set to 1 mV/s.

2.2.2 Electrochemical impedance spectroscopy (EIS)

The testing procedures for the EIS measurements were similar to those applied for the potentiodynamic polarization measurements. EIS experiments were conducted at the OCP using a Signal Recovery 5210 Analog Lock-in Amplifier under the frequency of 100 kHz–MHz with AC signals of 10-mV.

2.2.3 Surface analysis

The images of carbon-steel samples soaked in the studied solutions for 24 h were observed using SEM (LEO 1530VP).

2.2.4 Weight-loss measurements

Each coupon was scrubbed and rinsed with ultrapure water, swabbed with alcohol, and then finally immersed in alcohol for a few minutes. After that, the samples were placed on the filter paper, dried with cold air, and weighed. The steel bars were immersed in SCP solutions containing sodium lignosulfonate for 480 h. After that, the coupons were washed with ultrapure water to clean out the corrosion products, thoroughly cleaned with ultrapure water in an ultrasonic bath, air-dried, and then reweighed. After following the above steps, we were able to calculate the corrosion rate of carbon steel.

2.2.5 Potential-of-zero-charge (PZC) analysis

EIS measurements were conducted to indirectly estimate the value of PZC by applying different potentials [44]. The test system and the method of PZC analysis were similar to those applied for the EIS tests. The spectrogram was fit through the equivalent circuit employed in the reference to obtain the double-layer capacitance (C_{dl}) and plot the C_{dl}–E diagram[45]. The minimum C_{dl} value of the corresponding interval was the PZC value of the working electrode [46].

3. RESULTS AND DISCUSSION

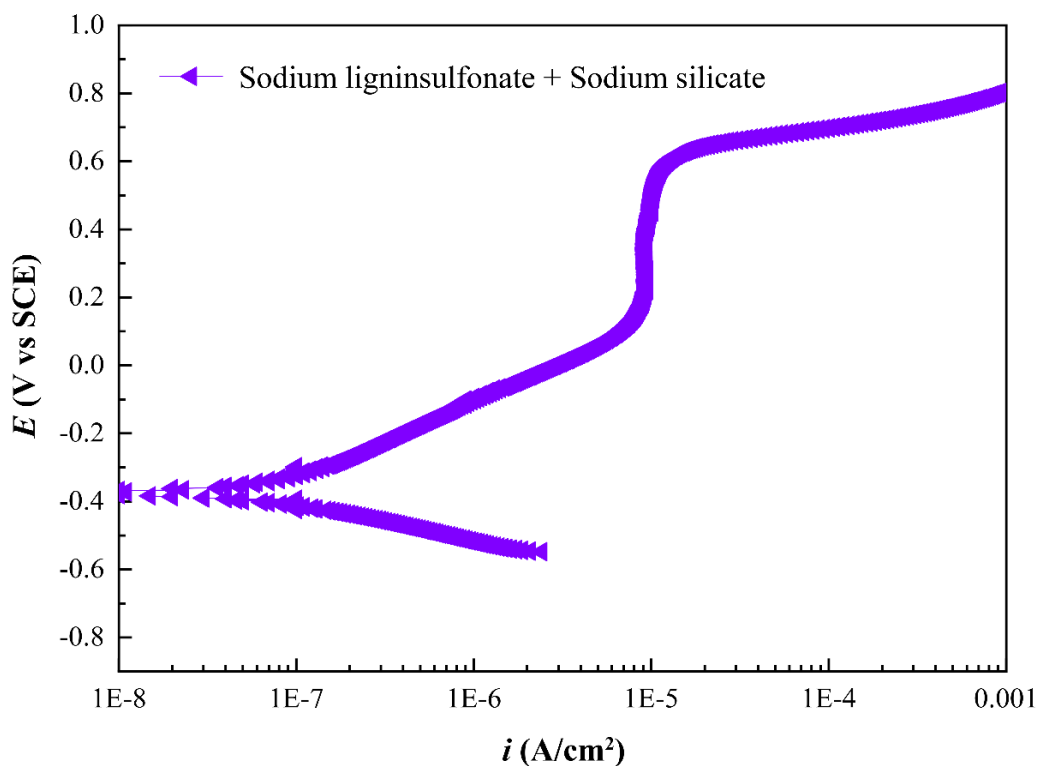### 3.1 Potentiodynamic polarization measurements

Fig. 1 presents the potentiodynamic polarization curves obtained in 0.08 mol/L NaCl saturated $Ca(OH)_2$ solution containing varying sodium lignosulfonate concentrations (i.e., 0, 0.0001, 0.0005,

0.001, and 0.0015 mol/L). Table 1 lists the corrosion parameters fitted from polarization plot via Tafel extrapolation. The inhibition efficiency (IE%) was evaluated using Eq. (1)[47] :

$$IE = [i_{corr}(blank) - i_{corr}(\text{adding inhibitor})]/i_{corr}(blank) \tag{1}$$
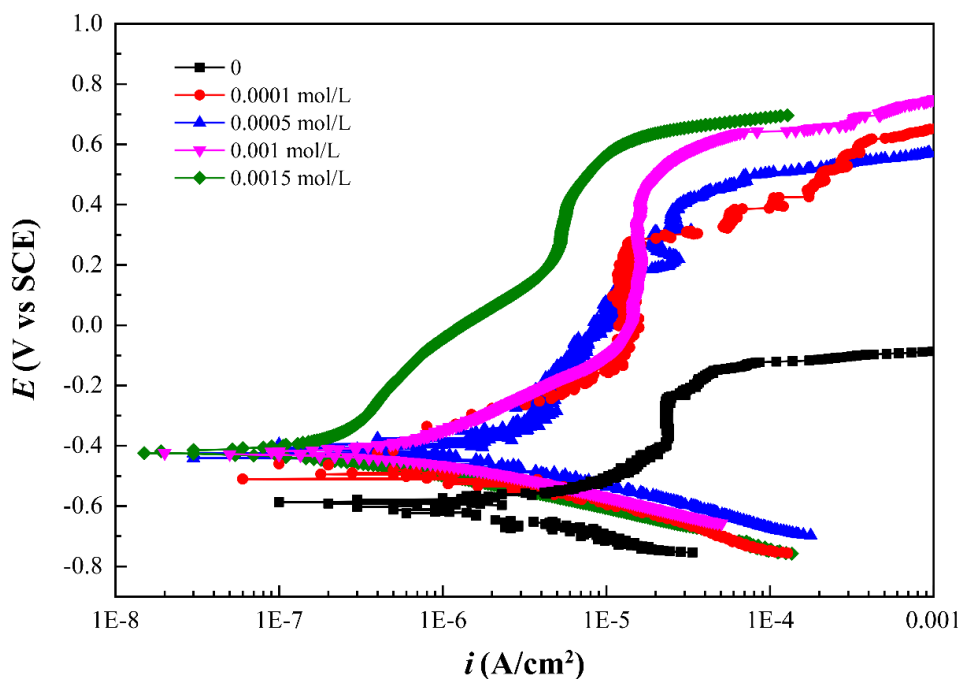
Figure 1. Potentiodynamic polarization curves under the influence of various concentrations of sodium lignosulfonate in a test solution.

Figure 2. Effect of compound inhibitor on the potentiodynamic polarization plot of Q235 steel in 0.08-mol/L NaCl-saturated calcium hydroxide solution.

Table 1. Influence of the concentration of sodium lignosulfonate and composite inhibitor on the E_{corr}, i_{corr}, E_b, and IE% values of a carbon-steel electrode in a test solution.

Inhibitor	Concentration (mol/L)	E_{corr} (V)	i_{corr} (A·cm^{-2})	E_b (V)	IE%
Blank	0	−0.591	9.18×10^{-6}	−0.231	-
Sodium lignosulfonate	0.0001	−0.503	1.12×10^{-6}	0.284	87.8
	0.0005	−0.427	8.80×10^{-7}	0.423	90.4
	0.001	−0.423	7.05×10^{-7}	0.573	92.2
	0.0015	−0.402	3.90×10^{-7}	0.626	95.8
Sodium lignosulfonate + sodium silicate	0.0005+0.0005	−0.372	1.11×10^{-7}	0.620	98.8

The curves in Fig. 1 shows that the corrosion current density value (i_{corr}) is mainly controlled by the polarizability of the anode. Sodium lignosulfonate has greater influence on anodic reaction. With the addition of all studied concentrations of sodium lignosulfonate, the anodic branch of the polarization curve further shifted left, while the i_{corr} value decreased and the corrosion potential (E_{corr}) value gradually improved. These observations are due to the inhibition of sodium lignosulfonate on the anode reaction of the metal and better resistance on the electrode process of the anode. As the sodium lignosulfonate concentration increases,the breakdown potential (E_b) value shifts to positive and the passivation range obviously widen. Adding 0.0015-mol/L sodium lignosulfonate resulted in a rapid decline in the anodic reaction rate and a shift in the E_{corr} value toward the positive direction. Upon increasing the sodium lignosulfonate concentration to 0.0015 mol/L, the anodic portion of the curve clearly shifted toward the left and the anodic reaction rate remarkably decreased.

The results of comparison of the anticorrosion properties of sodium lignosulfonate and other inhibitors are listed in Table 2. Sodium lignosulfonate exhibits better inhibition performance at low concentration.

Table 2. Comparison of the inhibition rate of sodium lignosulfonate and other inhibitors.

Corrosion Inhibitor	Test Solution	Concentration	IE%	Reference
Maize gluten meal extract	3% NaCl + Saturated calcium hydroxide solution	2 g/L	88.1	[48]
Phytic acid	1-mol/L NaCl+ Saturated calcium hydroxide solution	5.3 mmol/L	94.22	[49]
New triazole	Simulated concrete solution with 3.5% NaCl	2 mmol/L	95.5	[50]
Internal blending organic inhibitor	3.5% NaCl+ Saturated calcium hydroxide solution	4%	89	[51]
N,N'-Dimethylaminoethanol	Simulated concrete solution with 0.5-mol/L NaCl	0.125 mol/L	80	[52]

Potentiodynamic polarization experiments were performed upon addition of sodium silicate (0.0005 mol/L) and sodium lignosulfonate (0.0005 mol/L) on Q235 steel in a corrosive medium containing simulated concrete solution with 0.08-mol/L NaCl (Fig. 2). Both the cathodic and anodic current densities reduced in simulated chloride-contaminated concrete pore solutions containing the composite corrosion inhibitor; thus, sodium silicate combined with sodium lignosulfonate can be considered a mixed-type inhibitor. Fig. 2 displays that the combination of the two studied inhibitors increased the corrosion potential and expanded the passive region (between 0.164V and 0.620 V). When only sodium lignosulfonate was added, the passivation zone was not obvious and the breakdown potential reached 0.423 V. The value of the breakdown potential was found to be 0.620 V in the presence of the mixed-type inhibitor. This corresponds to an inhibition rate of 98.8%, which is given by Eq. (1).The use of sodium silicate as co-inhibitor resulted in an excellent passivation ability of carbon steel and a stable passive film compared to the use of sodium lignosulfonate alone.

3.2 Electrochemical impedance spectroscopy

EIS plots were obtained in SCP solutions at room temperature using different concentrations of sodium lignosulfonate as inhibitors for Q235 steel. The values extracted from the Nyquist plots for steel bar corrosion in SCP solutions with various contents of inhibitors are listed in Table 3. An equivalent circuit diagram was utilized to fit the impedance data via ZSimpWin software(Fig. 3). R_s is the solution resistance, R_{ct} represents the charge transfer, and CPE is the double layer capacitance (C_{dl}) of the metal/solution interface.In Fig. 4, Nyquist plots of carbon-steel electrode immersed in simulated concrete solution with various investigated inhibitor concentrations are displayed.
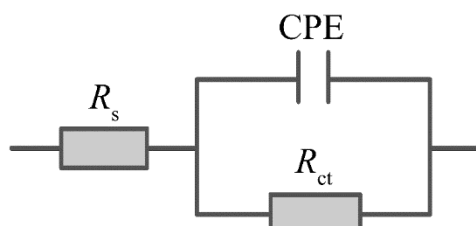

Figure 3. Equivalent circuit plot.

The charge-transfer resistance (R_{ct}) reflects the difficult degree of charge-transfer at the working electrode–solution interface during corrosion process. The larger R_{ct} value represents that the charge-transfer is more difficult, and, therefore, the corrosion rate becomes lower. A large capacitive semicircle denotes that the process of corrosion is concerned with the performance of double layer and charge-transfer process [53]. The Nyquist plots indicate that the larger the capacitive semicircle, the denser the generated inhibition film.The diameters of the capacitive arcs of samples in SCP solutions containing sodium lignosulfonate were larger than those in SCP solutions without inhibitor. For higher concentrations of sodium lignosulfonate in the SCP solution, a larger capacitive arc corresponds to an

increasing charge-transfer resistance. The inhibition rate improved with increasing sodium lignosulfonate concentration.
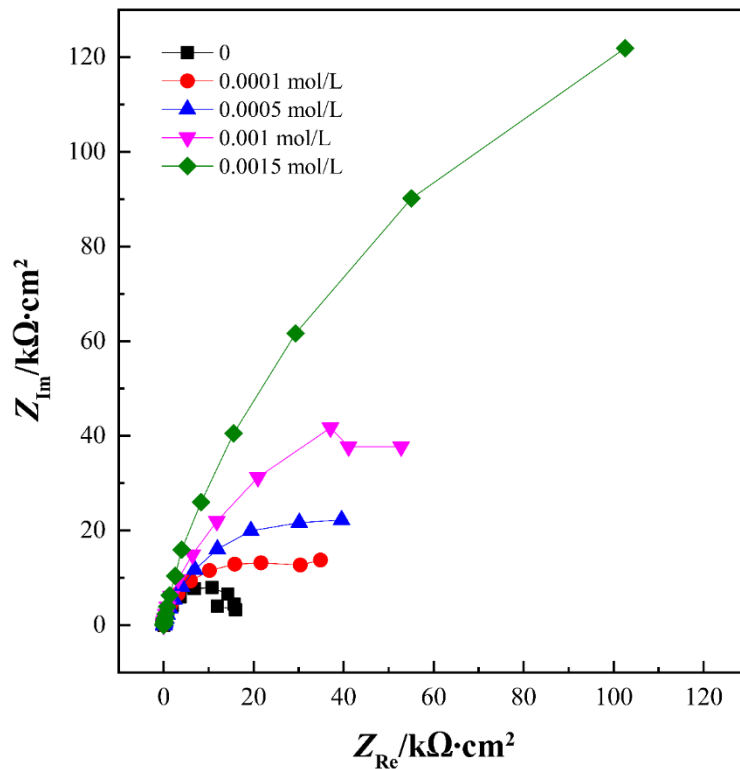
Figure 4. Nyquist curves of a carbon-steel electrode for different concentrations of sodium lignosulfonate in SCP solutions.
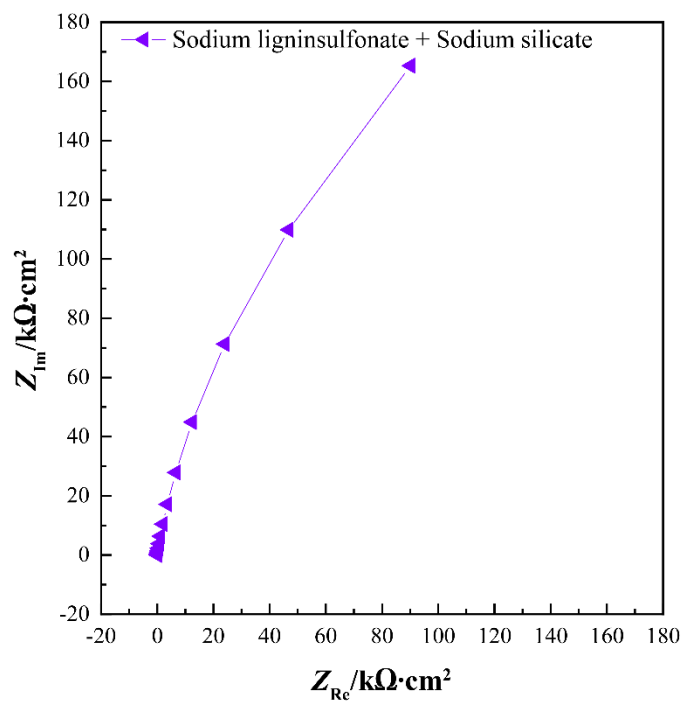
Figure 5. Influence of compound inhibitor on the Nyquist diagrams of samples in SCP solution.

Table 3. Impedance parameters for a carbon-steel electrode treated with sodium lignosulfonate with different concentrations and composite inhibitor.

Inhibitor	Concentration (mol/L)	R_s ($\Omega \cdot cm^2$)	Y_0 ($10^{-5}\Omega^{-1}\cdot cm^{-2}\cdot s^n$)	n	R_{ct} ($k\Omega \cdot cm^2$)
Blank	0	44.49	7.427	0.846	17.3
Sodium lignosulfonate	0.0001	8.38	7.801	0.862	34.1
	0.0005	6.99	7.171	0.876	48.9
	0.001	6.51	5.632	0.891	85.3
	0.0015	15.90	6.193	0.905	283.6
Sodium lignosulfonate + sodium silicate	0.0005 + 0.0005	44.9	5.70	0.896	272.1

Especially, upon increasing the sodium lignosulfonate concentration from 0.001 to 0.0015 mol/L, the capacitive arc radius increased considerably. The R_{ct} value rose from 85.3 to 283.6 k$\Omega \cdot cm^2$, that is, the inhibition efficiency of carbon steel substantially improved. The value of n represents the degree to which the double-layer capacitance of the Q235 steel electrode deviates from the ideal capacitance. The value of n is between 0 and 1. CPE is pure resistance when n is equal to zero. CPE represents pure capacitance when n is shown to be one[54].It is worth mentioning that the value of n was found to increase with increasing concentrations of sodium lignosulfonate in test solutions. At the optimal sodium lignosulfonate concentration of 0.0015 mol/L, the value of n reached approximately 1, which illustrates that steel-electrode can considered close to pure capacitance. The excellent inhibition effect was observed at the highest tested concentration (i.e., 0.0015 mol/L). These findings are consistent with the potentiodynamic polarization test results.

The EIS technique was applied to investigate the mechanism of corrosion resistance by sodium silicate and sodium lignosulfonate on Q235 steel (see Fig. 5). Fig. 5 depicts that the EIS spectrum obtained with the mixed-typed inhibitor had the largest diameter of the capacitive reactance loop, further demonstrating that this inhibitor performed better. After the addition of the mixed-typed inhibitor, the maximum R_{ct} value was 272.1 k$\Omega \cdot cm^2$,see Table 3 . The results of the EIS studies and the polarization curves show that the presence of sodium silicate and sodium lignosulfonate leads to an optimal corrosion inhibition.

The metal/solution interface can be considered as the metal and solution forming a double layer with opposite charges. If the binding force between the metal ions and the inhibitor ions is greater than the hydration force between the metal ions and the water molecules, the adsorbed inhibitor molecules exist on the metal surface in solution, which become the internal double layer. The electrostatic interaction exists between the water molecules and the steel,so the water molecules form the outside double layer.The permittivity of the inhibitor ions is much lower than that of the water molecules, and the internal double layer is thicker than the outer layer. Therefore, a decrease in the capacitance of the double layer in the SCP solution was also observed because of the presence of the inhibitor. It can be concluded that the thicker the internal double layer, the lower the capacitance of the double layer. From Table 3 ,the addition of sodium lignosulfonate to the SCP solution can remarkably change the structure

between the metal and the solution, significantly reducing the double layer capacitance. Many inhibitor molecules—instead of water molecules—exist on the steel surface [55].

3.3 Surface analysis

The surface structures of the samples soaked in the simulated solutions for 24 h were monitored by SEM. The microscopy images of steels exposed to the simulated solutions without inhibitor and with 0.0005-mol/L sodium lignosulfonate as well as 0.0005-mol/L sodium lignosulfonate plus 0.0005-mol/L sodium silicate are shown in Figs. 8 a, b, and c. The steel was covered with corrosion products and suffered from severe pitting corrosion because of the existence of chlorides after 24 h immersion (see Fig. 6a). In other words, the initiation and growth of pits destroyed the protective film. However, there was less corrosion damage on the steel treated with 0.0005-mol/L sodium lignosulfonate (Fig. 6b). The smoothness of the surface increased, but the film formed in sodium lignosulfonate at this concentration was not protective enough. The mixed-type inhibitor makes the passivation film completely smooth and more continuous, as shown in Fig. 6c. A few pits are observed but there are still no corrosion products. These results reveal that the mixed-type inhibitor effectively hinders the ingress of Cl$^-$ into the protection layer.
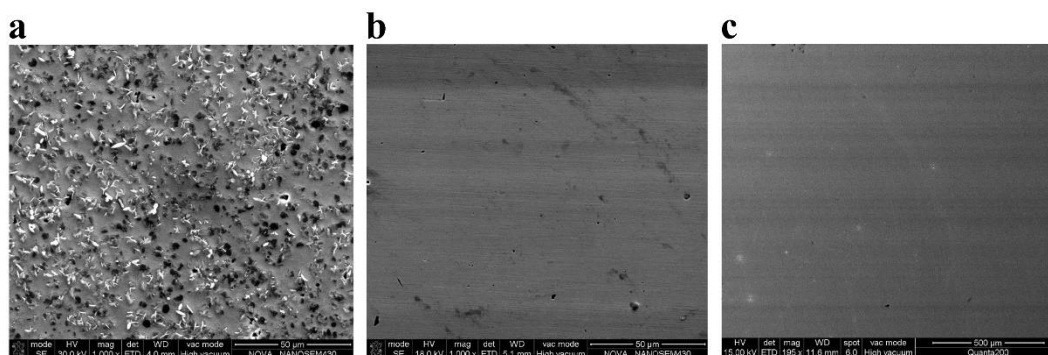
Figure 6. SEM images of carbon-steel coupons (a) in blank, (b) immersed in an SCP solution containing sodium lignosulfonate, and (c) immersed in an SCP solution containing sodium lignosulfonate and sodium silicate.

3.4 Weight-loss measurements

Weight-loss methods were conducted on Q235 carbon-steel in SCP solutions containing various concentrations of sodium lignosulfonate, namely, 0.0001, 0.0005, 0.001, and 0.0015 mol/L. Each sample was weighed before being completely soaked in the simulated solution for a period of 480 h. The corrosion rates inhibition efficiency can be assessed from the following formulas. The weight-loss results are presented in Table 4.

$$V = \frac{87600 \times \triangle W}{St\rho} \qquad (2)$$

$$IE = \frac{V_0 - V_t}{V_0} \times 100\% \qquad (3)$$

where ΔW is the average loss quality of the sheet (g).S is the total area of the sample (28 cm^2). t is the exposure time (480 h). ρ is the density of the sheet (7.85 g/cm^3). V_0 and V_t are the corrosion rates of specimen in the blank solution and the simulated solution with inhibitor, respectively.

The sodium lignosulfonate studied in this work is a good corrosion inhibitor, particularly with increasing concentration. Compared with other concentrations of sodium lignosulfonate, it is found to be the best inhibitor with an IE of 97.1% at a concentration of 0.0015 mol/L.

Table 4. Weigh-loss experimental parameters of Q235 steel treated with disparate concentrations of sodium lignosulfonate in SCP solutions.

Concentration (mol/L)	Corrosion Rate(mm/a)	IE%
0	1.16×10^{-2}	-
0.0001	1.60×10^{-3}	86.2
0.0005	6.06×10^{-4}	94.8
0.001	5.07×10^{-4}	95.6
0.0015	3.39×10^{-4}	97.1

3.5 PZC measurements

The factors affecting the adsorption properties of corrosion inhibitors include the existing form of corrosion inhibitors in solution, molecular structure, and electric charge on working electrode surface [56]. The corrosion inhibitor has an impact on the amount of charge at the electrode interface. The value of the PZC corresponds to the corrosion kinetics. The surface charge of the steel can be acquired from the OCP (E_{ocp}) with respect to PZC ($E_{q=0}$)[57].The Q235 steel surface charge at E_{ocp} can be calculated from Eq. (4) [58]:

$$E_r = E_{ocp} - E_{q=0} \qquad (4)$$

where E_r represents the rational corrosion potential of Antropov. When E_r is positive, the steel surface is positively charged and induces the adsorption of anions. In contrast, when E_r is negative, cation adsorption is favored.

EIS tests were measured in the potential scanning from -700 to -450 mV and from -550 to -300 mV in simulated solutions without and with 0.0005-mol/L sodium lignosulfonate. The obtained C_{dl}–E diagram is shown in Fig. 7. In the curve, the potential corresponding to the minimum capacitance refers to $E_{q=0}$[46]. Table 5 shows the parameters of PZC. According to Table 5, the values of OCP in the blank and inhibited solutions are -591 and -427 mV, respectively. The PZC values of the carbon-steel electrode should be -607 and -318 mV in 0.08-mol/L NaCl, saturated calcium hydroxide solution without and with sodium lignosulfonate, respectively.

Table 5. Parameters of the potential of zero charge.

Corrosion Inhibitor	Polarization Value	E_{ocp} (mV)	$E_{q=0}$ (mV)	Electrified Condition
Blank	−700 to −450 mV	−591	−607	Positive Charge
Sodium Lignosulfonate	−550 to −300 mV	−427	−318	Negative Charge
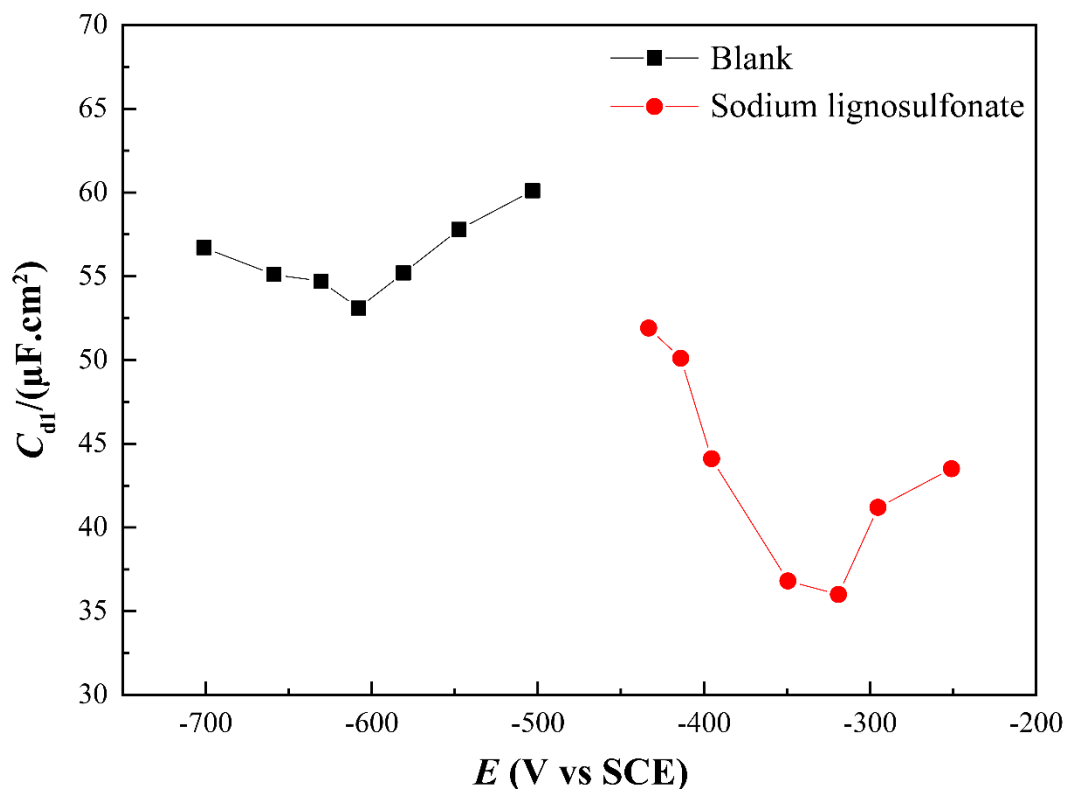
Figure 7. Plot of C_{dl} versus the applied electrode potential in simulated solutions in the absence and presence of 0.0005-mol/L sodium lignosulfonate.

The E_{ocp} value of carbon steel was greater than the $E_{q=0}$ value in the inhibitor-free simulated concrete pore solution; the carbon steel surface was positively charged. Carbon steel forms a passivation film in highly alkaline environments. OH^- and Cl^- ions show a strong competitive adsorption effect in SCP solutions, so they tend to adsorb easier on the metal surface. Particularly, the Cl^- ions are prone to adsorb on the grain-boundary of the passivation film—or on other defects—because of their high activity, small size, and strong electronegativity. It is found that positive charges exist on the surface, that is, positively charged ions (Ca^{2+}, Fe^{2+}, and Fe^{3+})adsorb on the passivation film. The electrostatic attraction between positive and negative ions is one of the driving forces of the inhibitor.

After adding sodium lignosulfonate to the SCP solution, the E_{ocp} value of carbon steel was lower than the $E_{q=0}$ value because of the extra negative charges on the metallic surface. In the test solution, the negative charges were lignosulfonate ions(LS^-), OH^- ions, and Cl^- ions. It is found that the charge density of the carbon steel was significantly different in various pH value conditions. In a solution with pH > 10, the sodium lignosulfonate surface shows a negative zeta potential.Its zeta potential shifts negatively with the rise of the PH.Sodium lignosulfonate is a spherical molecule, and its surface possesses negative charges in SCP solution (pH = 12.5) [59]. Therefore, the electrostatic attraction between sodium lignosulfonate and the positively charged carbon steel prompts sodium lignosulfonate to adsorb on the metal surface. Less chloride ions existing on the passive film demonstrates that the sodium lignosulfonate preferentially adsorbs on the metal surface. The surfaces of the samples were negatively charged owing to the adsorption of more sodium lignosulfonate, while the value of C_{dl} decreased at the same time [60].

3.6 Mechanism of inhibition

There are extra positive charges in the test solution because of the immersion of Q235 steel. The penetration of chloride ions on the carbon steel leads to formation of unstable ligands through Coulomb force. Sodium lignosulfonate instantly dissociates into sodium ions (Na^+) and lignosulfonate ions (LS^-).With the addition of inhibitor ions (LS^- and SiO_3^{2-}) ,these molecules precipitate on the surface and hinder the invasion of Cl^-,thus protecting the carbon steel [61]. Moreover, the oxygen in phenolic hydroxyl and carboxyl of sodium lignosulfonate shares the unshared pair of electrons with the empty d_{sp} orbital of the metal and generates an adsorbent layer.The lignosulfonate molecules that contain the benzene rings with multiple substituents cause the increasing electron cloud density and form a coordinate bond, which chemically absorb on the surface [62, 63]. Thus, sodium lignosulfonate can be considered an adsorption inhibitor.

Adding sodium silicate to an SCP solution can enhance the pH value of the solution. The $Fe(OH)_3$ and subsilicate are deposited on the carbon steel, so oxygen experiences a barrier effect in reaching the cathode, which prevents cathodic reaction from occurring [29]. With an increase in silicon content, silicate compounds ($Fe_2(SiO_3)_3$) may be preferentially deposited on the defects of the passive film, thus improving its self-repairing ability [64]. After sodium silicate completely dissolves in water, it forms colloidal particles ($[mSiO_2 \cdot nH_2O \cdot pSiO_3]^{-2p}$) with negative charges, which have a strong affinity for the corrosive product (FeOOH) on the steel surface.These colloidal particles may react with FeOOH to form a ferrosilicon protection film. Furthermore, colloidal cations are created owing to the presence of large amounts of Ca^{2+} and SiO_3^{2-} species in the SCP solution. A dense precipitation film is generated via electrostatic attraction between the colloidal cations and sodium lignosulfonate.

4. CONCLUSIONS

(i) The parameters determined from the fitting of the polarization plots show that the inhibition efficiency of an SCP solution containing sodium lignosulfonate reaches 95.8% while the incorporation of sodium silicate and sodium lignosulfonate to the SCP solution could enhance the protection efficiency up to 98.8%.

(ii) Nyquist plots reveal that the size of the capacitive arcs increases in SCP solutions with different inhibitors. The radius of the capacitive arcs follows the order: sodium lignosulfonate + sodium silicate > sodium lignosulfonate > blank. This proves that the inhibition performance of various inhibitors on carbon-steel surfaces gradually improves, and that the mixed-type inhibitor leads to the best corrosion resistance.

(iii) SEM images of the carbon-steel samples show that the film flatness in the following order: sodium lignosulfonate + sodium silicate > sodium lignosulfonate > blank.

(iv) Weight-loss measurements reveal that the inhibition rate gradually enhances with a rise in sodium lignosulfonate concentration.

(v) Zero-charge-potential measurements suggest that the sodium lignosulfonate adsorbs chemically on the Q235 steel surface, thereby improving the corrosion resistance of Q235 steel.

References

1. C. Chen, L. Jiang, M.-Z. Guo, P. Xu, L. Chen and J. Zha, *Constr. Build. Mater*., 228 (2019) 116752.
2. M. G. Sohail, R. Kahraman, N. A. Alnuaimi, B. Gencturk, W. Alnahhal, M. Dawood and A. Belarbi, *Constr. Build. Mater*., 232 (2020) 117205.
3. A. James, E. Bazarchi, A. A. Chiniforush, P. P. Aghdam, M. R. Hosseini, A. Akbarnezhad, I. Martek and F. Ghodoosi,*Constr. Build. Mater*., 224 (2019) 1026.
4. W. Wang, Z. Song, M. Guo, L. Jiang, B. Xiao, Q. Jiang, H. Chu, Y. Liu, Y. Zhang and N. Xu, *Constr. Build. Mater*., 228 (2019) 116713.
5. S. Jiang , L. Jiang, Z. Wang, M. Jin, S. Bai, S. Song and X. Yan, *Constr. Build. Mater*., 150 (2017) 238.
6. S. M. Trépanier, B. B. Hope and C. M. Hansson, *Cem. Concr. Res*., 5 (2001) 713.
7. C. M. Hansson, L. Mammoliti and B. B. Hope, *Cem. Concr. Res*., 28 (1998) 1775.
8. C. Monticelli, A. Frignani and G. Trabanelli, *Cem. Concr. Res*., 30 (2000) 635.
9. S. A. Umoren and M. M. Solomon, *J. Environ. Chem. Eng.*, 5 (2017) 246.
10. A. Królikowski and J. Kuziak, *Electrochim. Acta*, 56 (2011) 7845.
11. A. Popova and M. Christov, *Corros. Sci*., 48 (2006) 3208.
12. H. E. Jamil, M. F. Montemor, R. Boulif, A. Shriri and M. G. S. Ferreira, *Electrochim. Acta.,* 48 (2003) 3509.
13. S. Y. Chen, B. Zhu and X. Liang, *Int. J. Electrochem. Sci.,* 15 (2020) 1.
14. X. Wang , H. Jiang, D. X. Zhang, L. Hou and W. J. Zhou, *Int. J. Electrochem. Sci*., 14 (2019) 1178.
15. H. Lgaz, S. Zehra, K. Toumiat, A. Chaouiki, Y. El Aoufir, I. H. Ali, M. I. Khan, R. Salgh and I. M. Chung, *Int. J. Electrochem. Sci*., 14 (2019) 6699.
16. Y. Liu, Z. Song, W. Wang, L. Jiang, Y. Zhang, M. Guo, F. Song and N. Xu, *J. Clean Prod*., 214 (2019) 298.
17. M. A. Asaad, M. Ismail, M. M. Tahir, G. F. Huseien, P. B. Raja and Y. P. Asmara, *Constr. Build. Mater*., 188 (2018) 555.
18. S. A. Asipita, M. Ismail, M. Z. A. Majid, Z. A. Majid, C. Abdullah and J. Mirza, *J. Clean Prod.*. 67 (2014) 139.

19. S. P. Palanisamy, G. Maheswaran, A. G. Selvarani, C. Kamal and G. Venkatesh, *J. Build. Eng.*. 19 (2018) 376.
20. R. Anitha, S. Chitra, V. Hemapriya, I.-M. Chung, S.-H. Kim and M. Prabakaran, *Constr. Build. Mater.*, 213 (2019) 246.
21. I. Pradipta, D. Kong and J. B. L. Tan, *Constr. Build. Mater.*, 221 (2019) 351.
22. V. K. Thakur, M. K. Thakur, P. Raghavan and M. R. Kessler, *ACS Sustain. Chem. Eng.*, 2 (2014) 1072.
23. S. Liu, Z. Lin, Z. Cai, J. Long, Z. Li and X. Li, *Bioresour. Technol.*, 264 (2018) 382.
24. J. D. Megiatto, Jr., B. M. Cerrutti and E. Frollini, *Int. J. Biol. Macromol.*, 82 (2016) 927.
25. J. Ma, M. A. Khan, M. Xia, C. Fu, S. Zhu, Y. Chu, W. Lei and F. Wang, *Int. J. Biol. Macromol.*, 138 (2019) 188.
26. L. H. Grierson, J. C. Knight and R. Maharaj, *Cem. Concr. Res.*, 35 (2005) 631.
27. M. Alexandri, H. Papapostolou, M. Komaitis, L. Stragier, W. Verstraete, G. P. Danezis, C. A. Georgiou, S. Papanikolaou and A. A. Koutinas, *Bioresour. Technol.*, 214 (2016) 504.
28. T. Aro and P. Fatehi, *ChemSusChem*, 10 (2017) 1861.
29. B. Lin and Y. Zuo, *Molecules*, 24 (2019) 518.
30. E. C. Petrou and C. P. Pappis, *ACS Sustain. Chem. Eng.*, 2 (2014) 2527.
31. M.-r. Yuan, J.-t. Lu and G. Kong, *Surf. Coatings Technol.*, 204 (2010) 1229.
32. E. Akbarzadeh, M. N. M. Ibrahim and A. A. Rahim, *Corros. Eng. Sci. Technol.*, 47 (2012) 302.
33. F. Wang, J. Yu, Z. Zhang, Y. Xu and R.-a. Chi, *Process Saf. Environ. Prot.*, 117 (2018) 511.
34. A. A. Olajire, *J. Mol. Liq.*, 269 (2018) 572.
35. M. Kazemi, I. Danaee and D. Zaarei, *Mater. Chem. Phys.*, 148 (2014) 223.
36. R. Farid, K. Rajan and D. K. Sarkar, *Surf. Coatings Technol.*, 374 (2019) 355.
37. B.-l. Lin, J.-t. Lu and G. Kong, *Surf. Coatings Technol.*, 202 (2008) 1831.
38. X. Q. Xinping Ouyang, H. Lou and D. Yang, *Mater. Interfaces*, 45 (2006) 5716.
39. L. A. de Oliveira, O. V. Correa, D. J. dos Santos, A. A. Z. Páez, M. C. L. de Oliveira and R. A. Antunes, *Corros. Sci.*, 139 (2018) 21.
40. R. Ramanauskas, O. Girčienė, L. Gudavičiūtė and A. Selskis, *Appl. Surf. Sci.*, 327 (2015) 131.
41. R. F. Zhang, S. F. Zhang, J. H. Xiang, L. H. Zhang, Y. Q. Zhang and S. B. Guo, *Surf. Coatings Technol.*, 206 (2012) 5072.
42. M.-R. Yuan, J.-T. Lu, G. Kong and C.-S. Che, *Surf. Coatings Technol.*, 205 (2011) 4466.
43. O. Lopez-Garrity and G. S. Frankel, *Electrochim. Acta*, 130 (2014) 9.
44. R. Solmaz, M. Mert, G. Kardas, B. Yazici and M. Erbil, *Acta Physico Chim. Sin.*, 24 (2008) 1185.
45. G. Trabanelli, C. Monticelli, V. Grassi and A. Frignani, *Cem. Concr. Res.*, 35 (2005) 1804.
46. X. H. Xie, E. L. Li and Z. K. Tang, *Int. J. Electrochem. Sci.*, 5 (2010) 1018.
47. N. K. Othman, S. Yahya and M. C. Ismail, *J. Ind. Eng. Chem.*, 70 (2019) 299.
48. Z. Zhang, H. Ba and Z. Wu, *Constr. Build. Mater.*, 227 (2019) 117080.
49. F. Cao, J. Wei, J. Dong and W. Ke, *Corros. Eng. Sci. Technol.*, 53 (2018) 283.
50. Z. Zhang, F. Wang, Y. Liu, S. Wu, W. Li, W. Sun, D. Guo and J. Jiang, *RSC Adv.*, 8 (2018) 20648.
51. P. Wang, Y. Wang, T. Zhao, C. Xiong, P. Xu, J. Zhou and Z. Fan, *J. Adv. Concr. Technol.*, 18 (2020) 116.
52. M. Hassoune, A. Bezzar, L. Sail and F. Ghomari, *J. Adhes. Sci. Technol.*, 32 (2018) 68.
53. X. H. Li and X. G. Xie, *J. Taiwan Inst. Chem. Eng.*, 45 (2014) 3033.
54. L. Hamadou, A. Kadri and N. Benbrahim, *Appl. Surf. Sci.*, 252 (2005) 1510.
55. B. Lin, *Int. J. Electrochem. Sci.*, 14 (2019) 8080.
56. J. Zhao and G. Chen, *Electrochim. Acta*, 69 (2012) 247.
57. H. Ashassi-Sorkhabi, E. Asghari and P. Ejbari, *Acta Chim. Slov.*, 58 (2011) 270.
58. A. O. Yuce, R. Solmaz and G. Kardas, *Mater. Chem. Phys.*, 131 (2012) 615.
59. B. O. Myrvold, *Ind. Crops Prod.*, 27 (2008) 214.
60. M. Yamaguchi, H. Nishihara and K. Aramaki, *Corros. Sci.*, 36 (1994) 241.

61. Y. Wang, Y. Zuo, X. Zhao and S. Zha, *Appl. Surf. Sci*., 379 (2016) 98.
62. I. B. Obot, S. A. Umoren and N. K. Ankah, *J. Mol. Liq*., 277 (2019) 749.
63. A. A. Olajire, *J. Mol. Liq*., 248 (2017) 775.
64. K. Aramaki, *Corros. Sci*., 44 (2002) 1621.